Semiconductor Electrodes

X. Photoelectrochemical Behavior of Several Polycrystalline Metal Oxide Electrodes in Aqueous Solutions

Kenneth L. Hardee* and Allen J. Bard**

Department of Chemistry, The University of Texas at Austin, Austin, Texas 78712

ABSTRACT

An investigation was made of the photoelectrochemical properties of several polycrystalline metal oxide electrodes prepared by chemical vapor deposition, direct oxidation of the metal, or heating of suitable metal salt solutions. Further data are given on the behavior of the previously discussed TiO_2 and Fe_2O_3 electrodes including tunneling effects and the operation of the Fe_2O_3 in a solar cell. Other n-type materials studied were V_2O_5, WO_3, and PbO. WO_3 and PbO showed good anodic photocurrents but only WO_3 appeared stable. Bi_2O_3 showed both n- and p-type photocurrents, but had a poor stability. CuO produced a good cathodic photocurrent (indicating p-type behavior) with a photoresponse at wavelengths of 700 nm and below. Two other oxides, Cr_2O_3 and CoO, exhibited small p-type photoeffects.

Recent research on photosensitized reactions at semiconductor electrodes, aimed toward the photodecomposition of water and the construction of photogalvanic cells for use in solar energy conversion devices, has prompted investigations of new electrode materials. Suitable electrodes should be easily prepared and inexpensive, show stable behavior in use over long time periods of operation, and have a small bandgap (E_g) to allow efficient utilization of the solar energy spectrum. Most investigations to date have centered upon the more familiar semiconductor compounds, *e.g.*, Si, GaAs, GaP, ZnO, CdS, and TiO_2, usually in the form of single crystals. Stable electrodes, such as TiO_2, are large bandgap materials ($E_g \geq 3$ eV), while materials with smaller gaps, *e.g.*, Si and CdS, tend to be unstable. Moreover, the high cost and difficulty of obtaining single crystals of other compounds have limited investigations of other materials. Recently, polycrystalline semiconductors, prepared, for example, by chemical vapor deposition, have been shown to be suitable electrode materials and to behave similarly to single crystal electrodes (1, 2). The use of polycrystalline materials allows investigation of a wider range of compounds and is also of interest in any practical utilization of semiconductor electrodes. We describe here the photoelectrochemical behavior of a number of semiconducting oxides prepared in polycrystalline form. Further details are given on the nature and behavior of polycrystalline TiO_2 and Fe_2O_3, which we discussed previously (1, 2). Other oxides that show photoelectrochemical effects are Bi_2O_3, WO_3, PbO_2, V_2O_5, and CuO. Several other polycrystalline oxides, *i.e.*, CdO, MnO_2, and SrO exhibited little or no photoeffects.

Experimental

Several different methods of preparation of the polycrystalline electrodes were employed (Table I). The chemical vapor deposition (CVD) (TiO_2, Fe_2O_3, V_2O_5, WO_3, CdO, Cr_2O_3, MnO_2) followed the procedure outlined previously (1, 2). The corresponding acetylacetonate served as the vapor source, except for W and Ti where WCl_6 and $Ti(O_2C_3H_7)_4$ were used. Pt-foil substrates were employed for all electrodes. Oxides could also be prepared by direct oxidation of the metal. Thus Bi_2O_3 and lead oxide electrodes were prepared by melting the metal and allowing a surface film to form by air oxidation, at *ca.* 450°C. Finally, oxide films were formed by painting a suitable salt solution on Pt foil and then heating in a flame. Electrodes of WO_3, CuO, manganese oxide, CdO, Cr_2O_3, and SrO were produced in this manner. All Pt substrate electrodes had a copper wire attached to the back of the Pt foil with indium solder and were then sealed in a glass tube with Apiezon wax or silicone rubber (Dow Corning).

The single crystal V_2O_5 was generously donated by Professor A. B. Scott of Oregon State University. A 0.3 cm^2 piece was used with two Ag paint (Ernest Fullam, Incorporated, Schenectady, New York) contacts and was mounted in silicone rubber. The current-voltage response between the two contacts indicated ohmic behavior. The hematite was obtained from David New-Minerals (Stevensville, Montana). Contact was made to an approximately 0.5-1 cm thick sample with Ag paint.

X-ray diffraction was done on a General Electric XRD-6 diffractometer. A Joel, Incorporated (Tokyo, Japan) scanning electron microscope was used for examining the electrode surfaces. All electrochemical measurements were performed with buffered Na_2SO_4

Table I. Preparation and properties of materials used in this study

Substance	Preparation*	Type	E_g**	V_{fb}***	Photocurrent†
TiO_2	CVD	n	3.0	0 5 (*i*)	Good, stable
Fe_2O_3	CVD	n	2 2	−0.1 (*ii*)	Good, stable
	SE	n	2 2	−0.1 (*ii*)	
V_2O_5	CVD	n	2.75	+0.54 (*i*)	Poor, unstable
	XTAL	n	2.75	+ 0 80 (*i*)	
WO_3	CVD	n	2.6	−0.4 (*ii*)	Good, stable
	SE	n	2.6	−0.2 (*ii*)	Good, stable
	DOM	n	2.6	−0.25 (*ii*)	Good, unstable
Bi_2O_3	DOM	n	2.8	−0.08 (*ii*)	Good, unstable
		p	2.8		Fair, unstable
PbO	DOM	n	2.8	−0.3 (*ii*)	Good, unstable
CuO	SE	p	1.7	+0.3 (*i*)	Good, unstable
Cr_2O_3	CVD	p	unknown	—	Poor, unstable
	SE				
CoO	CVD	p	unknown	—	Poor, unstable
	SE				
CdO	CVD	—	—	—	None
	SE				
MnO_2	CVD	—	—	—	None
	SE				
SrO	SE	—	—	—	None

* CVD = chemical vapor deposition, SE = evaporation of solution on substrate, DOM = direct oxidation of metal.
** E_g is estimated from the wavelength of the onset of the photocurrent.
*** (*i*) pH of 7, value estimated from potential of onset of photocurrent; (*ii*) pH of 9 (V *vs.* SCE).
† Good, fair, and poor refer to relative magnitude of photocurrent.

* Electrochemical Society Student Member.
** Electrochemical Society Active Member.
Key words: photoelectrochemistry, solar cells, photovoltaic cells, semiconductors.

solutions. A simple H-cell with separate auxiliary and working compartments and with a Pyrex window was used. A saturated calomel (SCE) was the reference electrode. Electrochemical equipment consisted of a Princeton Applied Research (PAR) Model 173 potentiostat, a PAR Model 175 universal programmer, and a Houston Instruments (Austin, Texas) Model 2000 omnigraphic X-Y recorder. Illumination was done with either the full output of a 450-W xenon lamp (Oriel Corporation, Stamford, Connecticut) or the output of a Model 7240 grating monochromator (Oriel Corporation). Absolute light intensity measurements were made using an EG&G Model 550 Radiometer (EG&G, Incorporated, Salem, Massachusetts). The current *vs.* wavelength curves were corrected for intensity variations by normalizing the spectral output of the lamp-monochromator system to 470 nm and using the resulting values to correct the measured photocurrent curves, shown by dotted i-λ curves.

Results and Discussion

Titanium dioxide.—As reported earlier (1), the current (i) *vs.* potential (E) curves for a CVD TiO_2 electrode are quite similar to those of single crystal rutile. Typical i-E and i *vs.* wavelength (λ) curves for a CVD TiO_2 electrode are shown in Fig. 1. Examination of the CVD electrode surface with a scanning electron microscope (SEM) reveals a uniform, smooth surface of polycrystalline material (Fig. 2). There are no grain boundaries visible, but there are numerous cracks across the surface which range up to 1000Å wide. These cracks probably form during the high temperature treatment the electrode is subjected to during preparation. An edge view of the surface, accomplished by cutting the electrode and polishing the edge, reveals layers of oxide corresponding roughly to the different deposition (3-5 layers). The cracks are visible along the surface but none appear to penetrate directly to the substrate. From this edge view, the total thickness of the oxide layer was measured as about 40 μm.

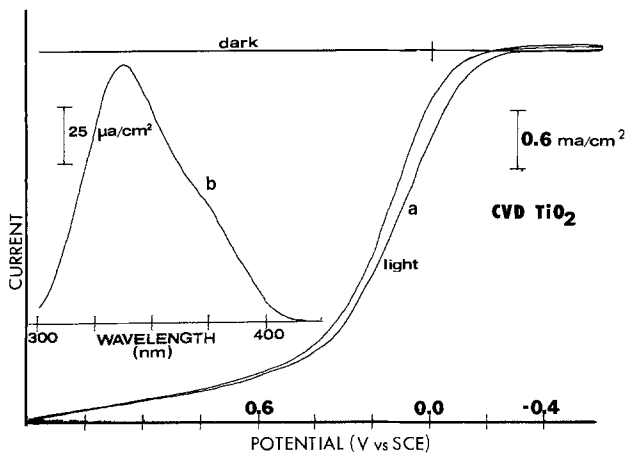

Fig. 1. (a) Current *vs.* potential curve for CVD TiO_2, 0.5M KCl, in dark and illuminated with Xe lamp. (b) Current *vs.* wavelength curve under same conditions, $E = +0.800$V *vs.* SCE.

X-ray diffraction patterns of the CVD TiO_2 electrode were typical powder patterns indicating polycrystalline material primarily in the rutile form of TiO_2. A small percentage ($\leq$ 10%) of anatase was also present. X-ray diffraction of an electrode that only had one coat of oxide deposited at about 150°C, but which was not heated further, revealed a pattern that was totally anatase. This electrode showed only a very low photocurrent. Thus the high temperature treatment is necessary not only to prevent flaking between coats and allow thicker coats to be deposited, but also to convert the film into the photoresponsive rutile form of TiO_2.

The thickness of the film on the electrodes affects the shape and magnitude of the photocurrent *vs.* potential curve. In Fig. 3 are given curves for several CVD TiO_2 electrodes prepared with increasing relative thicknesses (by depositing successive coats). As the film becomes thicker, the shape of the curve becomes more typical of a single crystal n-type semiconductor, exhibiting a sharper current rise and a more well-defined plateau. The effect of thickness on curve shape might be explained by the increasing absorbance of light in the space charge region (3). Alternately, the extent of recombination of electrons and holes might decrease with thickness as a more homogeneous film forms. The current *vs.* wavelength curves were similar for all of the electrodes.

The quantum efficiency of the CVD TiO_2 electrode is quite high in the plateau region. Typically, the quantum efficiency is $\geq$ 60% at the wavelength of maximum response (*ca.* 335 nm). Variations in the quantum efficiency from one electrode to another can be ascribed to variations in the thickness, as described above, and in the percentage of rutile actually present in the electrode.

As reported previously (1), at potentials of about 2.0V *vs.* SCE in neutral solutions (and at more nega-

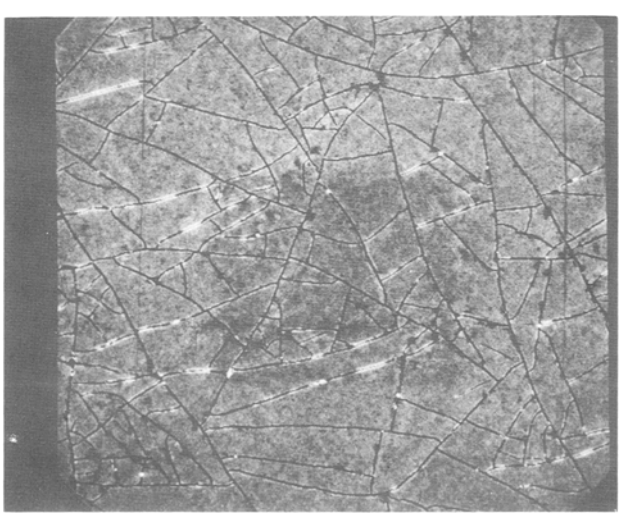

Fig. 2. Scanning electron micrograph of surface of CVD TiO_2. Magnification is 600×.

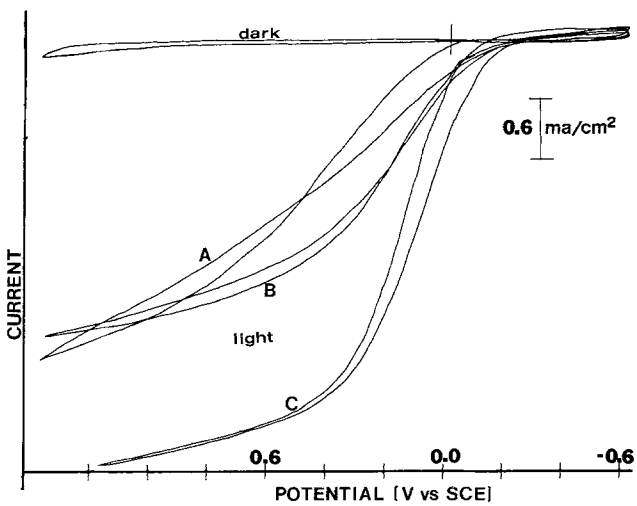

Fig. 3. Current *vs.* potential curves for CVD TiO_2 with varying relative thickness of film: (a) one 1 min coat, (b) two 2 min coats, (c) four 2 min coats.

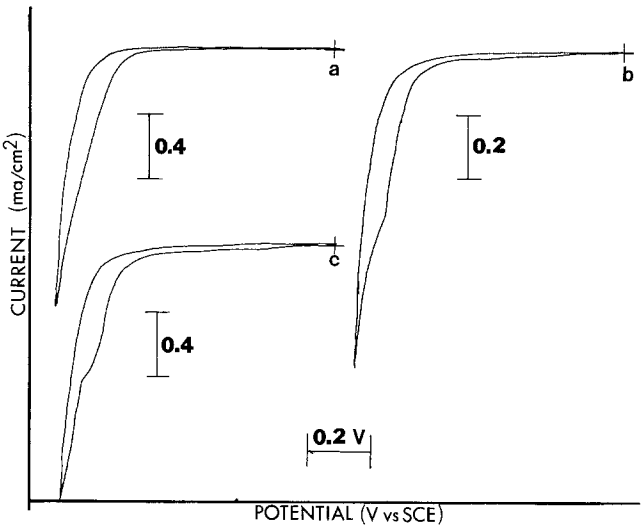

Fig. 4. Current *vs.* potential curves for CVD TiO_2 with addition of I^-: (a) 0.5M Na_2SO_4 (b) 0.5M Na_2SO_4 + 3.8 mM NaI, (c) 0.5M Na_2SO_4 + 7.5 mM NaI.

tive potentials at higher pH values), a large anodic current rise is observed in the dark for the CVD TiO_2 electrodes (Fig. 4a). Vigorous gas evolution is observed on the electrode surface. This current is attributed to tunneling of electrons from solution through the space charge region and into the conduction band. The narrow space charge region which is necessary for this tunneling is the result of the high doping level in the CVD TiO_2 electrode. For a single crystal electrode, appreciable anodic currents are usually not observed until potentials > 3V *vs.* SCE (16), depending, again, upon the doping level. The higher doping level in the CVD TiO_2 is the result of the more homogeneous reduction possible with thin films. The influence of a titanium substrate on the doping is apparently minimal, since similar effects are obtained with Pt substrates.

Addition of I^- to the solution produces a shoulder on the dark anodic current rise (Fig. 4b and c) with a height proportional to the concentration of I^-. The current is due to the oxidation of the I^-, and is similar to that observed on highly doped ZnO (6). The redox level of I^- lies nearer the flatband potential than the H_2O/O_2 level does. Thus the I^- is located where a narrower part of the space charge exists and electrons will tunnel at lower potentials, producing the observed curve. Addition of Br^- to the solution instead of I^- produced no noticeable addition to the tunneling current, since its level is near that of the H_2O/O_2 potential.

The behavior of CVD TiO_2 is fairly typical of an n-type semiconductor, with low anodic dark currents and well-defined anodic photocurrent plateaus. Because of the ease of doping of the thin films, they exhibit tunneling effects usually seen only at highly doped single crystal electrodes. With these properties, as well as its stability, CVD TiO_2 is useful as a comparison electrode in examining the behavior of the other oxide electrodes investigated in this study.

Iron oxide.—We have previously shown that iron oxide shows a good photoelectrochemical response at longer wavelengths in the visible region than that of TiO_2 (2). In that study we assumed, from the wavelength for the onset of the photocurrent, that the bandgap was about 2.2 eV, and from the procedure used in fabrication, that the oxide was Fe_2O_3. We have now examined the material with x-ray diffraction and a SEM. The results show that the film is primarily α-Fe_2O_3 (hematite), with a small amount of ζ-Fe_2O_3

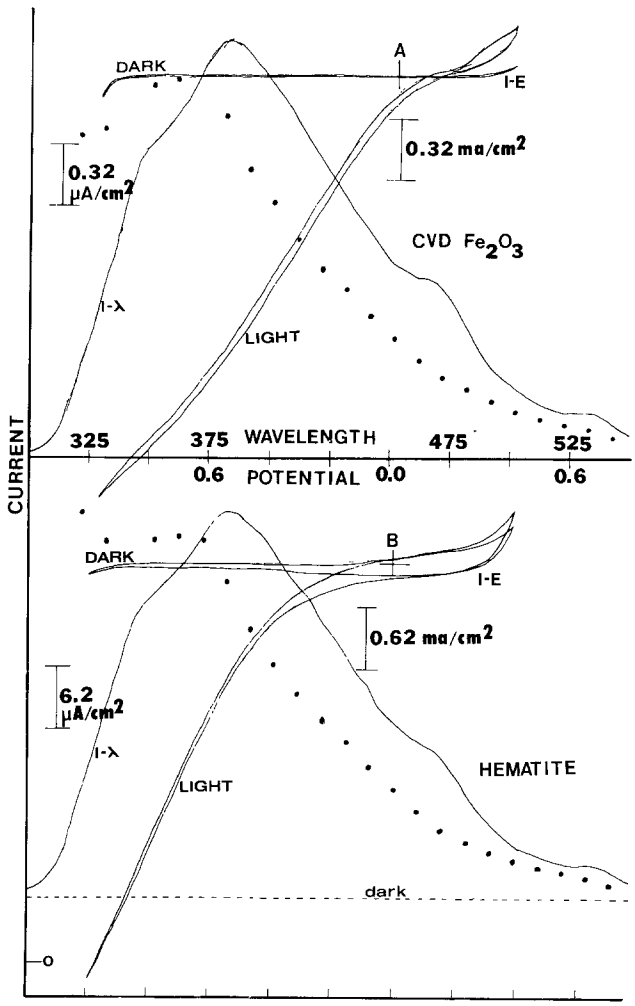

Fig. 5. Current *vs.* potential and current *vs.* wavelength curves for (a) CVD Fe_2O_3 in 0.25M Na_2SO_4, pH 9, (b) natural hematite in 0.5M Na_2SO_4. E = 0.600V *vs.* SCE for i-λ curves. Current scale for corrected i-λ curve is 2× uncorrected scale shown.

(*ca.* 20%) and γ-Fe_2O_3 (*ca.* 10%). The surface was very smooth with no visible cracks seen with the SEM for magnifications of 20,000×.

The i-E and i-λ curves for a CVD Fe_2O_3 electrode and a piece of natural hematite are shown in Fig. 5. The two i-λ curves are almost identical in shape, suggesting that the α-Fe_2O_3 form of the oxide is indeed the photoresponsive one.

Attempts made to deposit Fe_2O_3 on iron were unsuccessful, because the film flaked off during the high heat-treatment. Films on Pt which were not heated showed a very poor photoresponse, so the treatment is necessary to convert the film to α-Fe_2O_3 and make it n-type (7). Attempts at heating Fe_2O_3 on Fe in vacuum were also not successful, since the apparatus could not apparently achieve the required high temperatures (*ca.* 1200°-1400°C). Simply heating Fe plates until an oxide coating formed produced a slight photoresponse, but it was not nearly as large as that of CVD Fe_2O_3 on Pt, since, again, the formation of the required structure and doping levels could not be achieved without the oxide flaking off. CVD of the Fe_2O_3 was not necessary for good photoresponse, however. Electrodes made by heating a mineral oil slurry of the acetylacetonate or a solution of $FeCl_3$ in a flame on a Pt substrate showed good response. CVD does, however, allow better control of the reaction and thus more uniformity in the film, making it more useful for producing large area electrodes.

As with CVD TiO_2, the thickness of the film affects the shape and magnitude of the photocurrent *vs.* po-

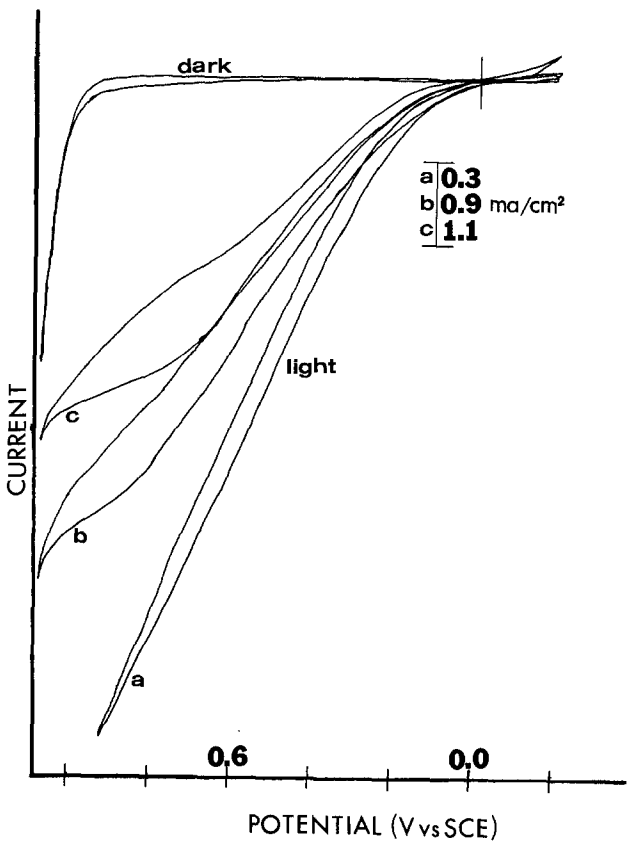

Fig. 6. Current *vs.* potential curves for CVD Fe_2O_3 of varying thicknesses in 0.25M Na_2SO_4 *p*H 9.2 solution: (a) 0.6 μm thick, (b) 1.7 μm thick, (c) 6.8 μm thick.

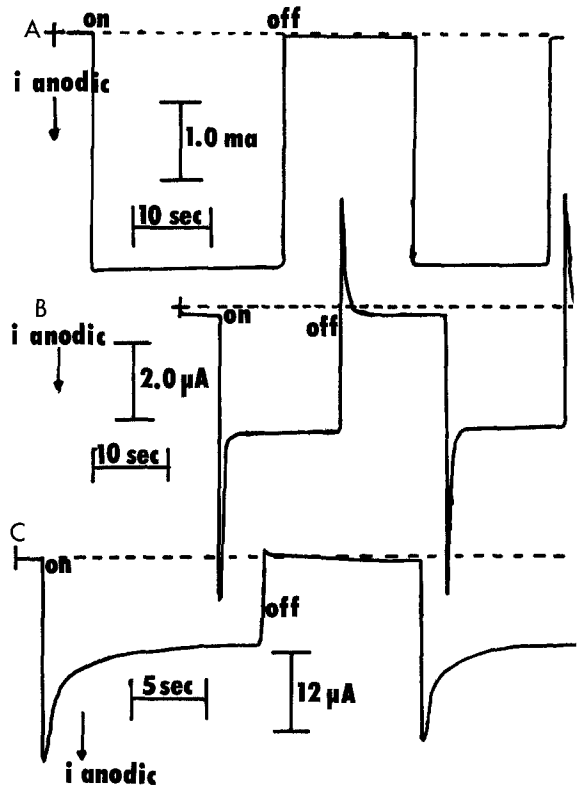

Fig. 7. Transient (*i-t*) curves in 0.25M Na_2SO_4 *p*H 9 for (a) CVD Fe_2O_3, white light, $E = 0.600$V; (b) CVD Fe_2O_3, monochromatic light, $\lambda = 375$ nm; (c) CVD TiO_2, $E = -0.300$V, $\lambda = 375$ nm.

tential curve (Fig. 6). The much lower anodic current observed on the return sweep is due to adherence of gas bubbles to the electrode surface. Tapping the electrode dislodges the bubbles and increases the current. Thicknesses were estimated by weighing the samples before and after deposition and assuming a density of 5.2 g/cm^3 for Fe_2O_3. For the thickest film twelve coats of Fe_2O_3 were chemically vapor deposited. (One coat equals approximately the amount required to cause no further changes in the interference color, *i.e.*, color becomes steady blue gray). As the film becomes thicker, a plateau region appears, but it never becomes as sharp as that for TiO_2. This indicates a greater recombination effect or lower absorptivity for the Fe_2O_3. Similar *i-E* curves were observed by depositing successive coats on the same electrode and making photocurrent measurements between coats.

The efficiency for the CVD Fe_2O_3 electrode depends, as does that for TiO_2, on the potential and wavelength. Photocurrent densities of the order of 6 mA/cm^2 have been obtained with Xe white light, which is comparable to that for TiO_2 with the same lamp. However, since Fe_2O_3 responds over a wider wavelength region, higher current densities would be expected. Thus the over-all quantum efficiency for Fe_2O_3 is somewhat lower than that of TiO_2. The transient photocurrent-time behavior found with Fe_2O_3 depends upon the light intensity and E and differs from that seen with CVD TiO_2 (Fig. 7). Under high illumination intensities (full Xe lamp output) no transient peaks are observed (curve a). When the intensity was decreased to about 1% of its level with a neutral density filter, a small anodic transient peak appears. At the very low light intensities of monochromatic light (curve b), sharp anodic transients were observed, with the steady photocurrent at these intensities being less than half of the peak value. When the light was turned off, a cathodic peak transient appeared. Similar behavior occurred at all wavelengths where Fe_2O_3 is responsive at similar light intensities (less than 1 mW/cm^2). Vigorous stirring of the solution had only a small effect on the steady current. Memming (8) observed a similar transient response at TiO_2. We have also observed this effect at CVD TiO_2; however, it occurs only on the rising portion of the *i-E* curve (Fig. 7c). On the plateau the transient for TiO_2 is like that for Fe_2O_3 in white light, with both intense white and weak monochromatic light. Notice that in the TiO_2 transient the cathodic peak occurring when the light is turned off is much smaller than the very small anodic one, while with Fe_2O_3 (Fig. 7b) the cathodic transient is of the order of one-half of the anodic one. As the potential is increased for TiO_2, the anodic transient remains well defined, disappearing on the plateau region.

This transient can be explained in terms of surface recombination or backreaction of the photogenerated species. Thus the oxygen (or hydroxyl radicals) which is produced by the photogenerated holes is thermodynamically reducible at potentials on the rising portion of the *i-E* curve. A backreaction between these and any electrons at the surface produces a backreaction [which is equivalent to a surface electron-hole recombination (3)] and a cathodic current component. This component decreases as the potential is made more positive, as expected. The effect of light intensity suggests that the extent of the backreaction is rather constant and independent of the intensity level, *e.g.*, reaching its maximum level when the surface is saturated with oxidized species. Thus, at high light intensities these transients are not observed. The results also suggest that this backreaction is more important for Fe_2O_3 than for TiO_2. The existence of this backreaction cathodic current can also be demonstrated by the following experiment. If the initial potential of a Fe_2O_3 electrode in the dark is set at $+0.80$V and scanned in a negative direction, a small cathodic current is observed at high sensitivity. Illuminating the electrode briefly and then scanning shows an increase

in this cathodic current due to the oxygen produced. Thus the quantum efficiency for photo-oxidation depends upon the light intensity, being smaller at lower intensities and giving anomalously low results for the monochromatic light. The effect of the backreaction is negligible, however, at the higher white (Xe) light intensities, since the transients are not observed under these conditions.

As with CVD TiO_2, Fe_2O_3 shows a large anodic current rise and gas evolution in the dark at potentials greater than about +1.2V. This probably represents tunneling of electrons into the conduction band. However, addition of I^- and $Fe(CN)_6^{4-}$ produced markedly different results at Fe_2O_3 than at TiO_2. The cyclic voltammetric curves for Fe_2O_3 and Pt electrodes of similar area with these species are shown in Fig. 8. For iodide oxidation E_{pa} at Fe_2O_3 is 0.417V, with a peak separation of 0.142V (compared to E_{pa} = 0.417V and ΔE_p of 0.118V at Pt). From simple area considerations, this anodic current for I^- oxidation at Fe_2O_3 cannot be due to exposed Pt under the Fe_2O_3. Neither does the SEM picture show cracks in the film. The curve for $Fe(CN)_6^{-4}$ is markedly different between Pt and Fe_2O_3. These results can be explained by a combination of conduction band and tunneling mechanisms. From the photocurrent *vs.* potential curves, the onset of photocurrent gives an estimate of the flatband potential. For Fe_2O_3 the flatband potential lies about 0.5V positive of that of TiO_2. This implies that the conduction band of Fe_2O_3 is 0.5 eV lower than that of TiO_2. Since the $E^{o'}$s for I^-/I_2 and $Fe(CN)_6^{-4}/Fe(CN)_6^{-3}$ are +0.54 and +0.35V *vs.* NHE, respectively, the redox levels of these couples must lie in the vicinity of the conduction band of Fe_2O_3. The near reversible behavior of the I^-/I_2 couple indicates that the overlap with the conduction band is quite good. The anodic current could be either tunneling or normal electron transfer at the conduction band edge. The $Fe(CN)_6^{-4}/Fe(CN)_6^{-3}$ curve appears irreversible with the anodic wave being almost a plateau. The cathodic wave is shifted in a negative direction but has a more diffusion-controlled shape. If the distribution functions of the $Fe(CN)_6^{-4}/Fe(CN)_6^{-3}$ couple are widely separated, such that $Fe(CN)_6^{-4}$ does not overlap well with the conduction band of Fe_2O_3, then the oxidation would proceed by tunneling and the reduction by a normal conduction band mechanism. The anodic wave is similar to that seen by Pettinger, Schoppel, and Gerischer (6) for Fe^{+2} at highly doped ZnO, which was interpreted as due to tunneling currents. Thus the Fe_2O_3 electrode must be highly doped, since it shows large anodic current rise in the dark, accompanied by gas evolution. The difference in behavior between Fe_2O_3 and TiO_2 can be ascribed to the higher lying conduction band in TiO_2, resulting in a poorer overlap with both the I^-/I_2 and $Fe(CN)_6^{-3}/Fe(CN)_6^{-4}$ distribution functions.

Fe_2O_3 solar cell.—A large (*ca.* 10 cm^2 area) Fe_2O_3 electrode was fabricated and operated in a solar cell arrangement with a fuel cell-air cathode similar to that of Laser and Bard for TiO_2 (4). In such a cell, oxygen is photogenerated at the Fe_2O_3 and is reduced at the fuel cell cathode, so that the net effect is conversion of light to electrical energy. Figure 9a gives the response curves (current, voltage, and power) for a typical cell with 1*M* NaOH electrolyte and irradiation with the Xe lamp. The potentiostatic *i-E* curves for this cell in the dark and under illumination are shown in Fig. 10. Maximum response of the electrode was achieved by focusing the light onto about 4 cm^2 of the electrode. The corresponding curves for operation in direct, unfocused sunlight are given in Fig. 11. If the sunlight was focused onto 1 cm^2 with a 10.5 cm diameter lens, currents of at least 8 mA could be achieved through a 1Ω load resistor. Vigorous gas evolution was observed from the illuminated spot. This Fe_2O_3 solar cell operated for more than 6 hr in unfocused sunlight and over 2 hr with the Xe lamp with no deterioration in response. Because the flatband potential of the Fe_2O_3 is rather positive, the output voltage and power of this cell are rather low. The current capabilities in the sunlight are quite good and suggest that it would be useful for solar decomposition of water in conjunction with a suitable p-type cathode.

The Fe_2O_3 solar cell was also operated using the I^-/I_2 reaction at a *p*H of about 9 with Xe lamp illumination (Fig. 9b). Initially no I_2 was present in the solution. After operation for a short time through a 1Ω load, the solution became yellow, indicating the production of I_2. The Fe_2O_3 electrode was very near

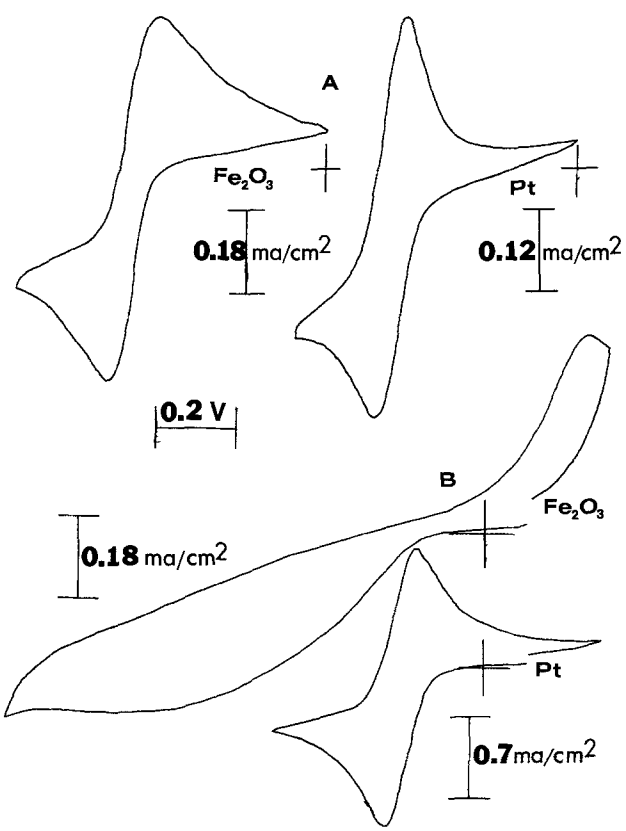

Fig. 8. (a) Cyclic voltammogram for CVD Fe_2O_3 and Pt in 0.5M Na_2SO_4 with 3.8 mM NaI. (b) Cyclic voltammogram for CVD Fe_2O_3 and Pt in 0.5M Na_2SO_4 with 7.5 mM $K_4Fe(CN)_6$.

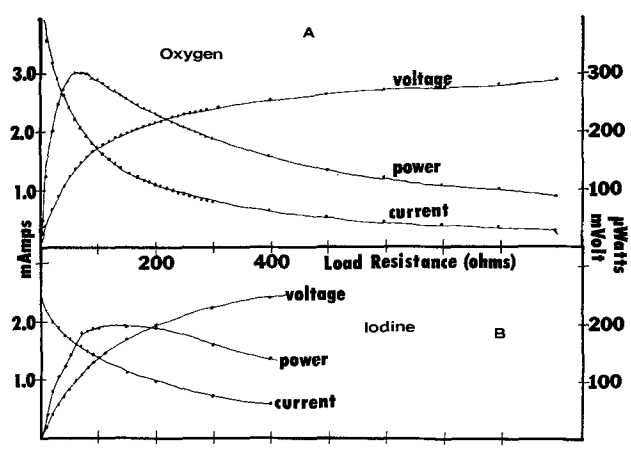

Fig. 9. Current, power, and voltage vs. load resistance for Fe_2O_3 solar cell. Xe lamp. (a) 1M NaOH, oxygen saturated; (b) 0.25M Na_2SO_4, *p*H 9, 33 mM NaI.

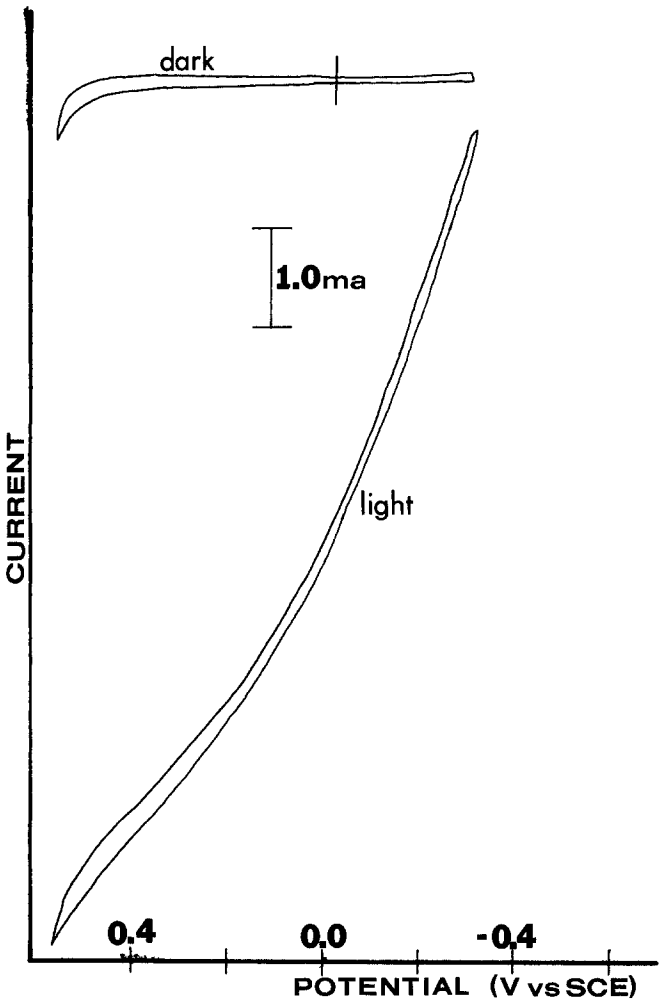

Fig. 10. Current *vs.* potential for Fe_2O_3 solar cell electrode in 1M NaOH.

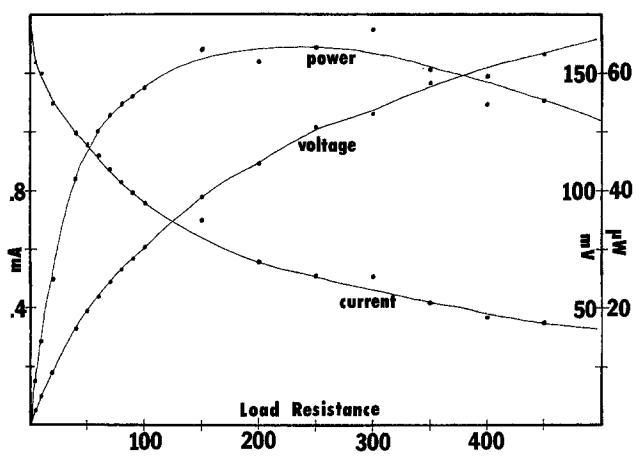

Fig. 11. Current, power, and voltage *vs.* load resistance for Fe_2O_3 solar cell, in 1M NaOH, oxygen saturated, direct sunlight.

the window, so the absorption of light by the I_2 was minimal. Prolonged bubbling of N_2 gas through the cell produced only a small decrease in the current. In contrast, during the operation of the cell without the I^-/I_2 couple, N_2 caused the current to decay ten times as fast, with the current finally approaching zero. The current was restored by bubbling O_2. Thus, the over-all solar cell reaction involves I^- oxidation at the Fe_2O_3 and I_2 reduction at the cathode. The rapid production of I_2 and the over-all effect on cell operation with I^- present indicate that the efficiency for photocatalytic generation of I_2 is relatively high, as it also is at TiO_2 (5). Thus Fe_2O_3 should work well and offer the advantage of longer wavelengths when used as an electrode for photoelectrosynthesis (5).

Bismuth oxide.—Photocurrents with anodic gas evolution were also observed at bismuth oxide electrodes prepared by heating bismuth metal; attempts at producing the oxide by CVD using $BiCl_3$ were unsuccessful. Typical *i-E* and *i-λ* curves in *p*H 8, Na_2SO_4 solution, with and without illumination, are shown in Fig. 12. There is a very low anodic and cathodic dark current (<0.1 $\mu A/cm^2$), although on the initial scan with a new electrode some anodic current was observed (dotted line), probably representing further oxidation of the surface. This current disappeared on subsequent scans. Scanning first in the dark to -0.4V *vs.* SCE did not result in any increase in the anodic dark current. With illumination both anodic and cathodic photocurrents are observed. The anodic photocurrent begins at approximately the same potentials as with Fe_2O_3 and exhibits a similar shape. Because of the method of preparation, the oxide film thickness could not be controlled easily, so that the effect of thickness on the *i-E* curve shape was not determined. Heating the sample longer (45 min *vs.* 2 min) produced lower photocurrents, but similar shapes. When the potential was held at $+0.60$V, gas evolution was observed during illumination. The photocurrent slowly decayed with time, unlike the behavior at TiO_2 or Fe_2O_3. After 1 hr of illumination, the photocurrent had decayed to about 0.4 its original value.

The maximum anodic photocurrent densities [*ca.* 1.6 mA/cm^2 with white (Xe) light] were obtained for Bi_2O_3 electrodes heated only a few minutes. Thus the over-all efficiency for photo-oxidation appears much less than that for TiO_2 or Fe_2O_3. After illumination, the electrode surface color had changed from an initial gray to yellow. The resistance of the electrode (measured with an ohmmeter between the surface and the contact) remained of the order of a few ohms. Dark currents before and after illumination also remained low.

Examination of the electrode surface by x-ray diffraction reveals the presence of two forms of Bi_2O_3, and α- and γ-forms. The relative amount of the two forms was dependent on the length of time the Bi sample was heated. After heating 3-5 min the α:γ

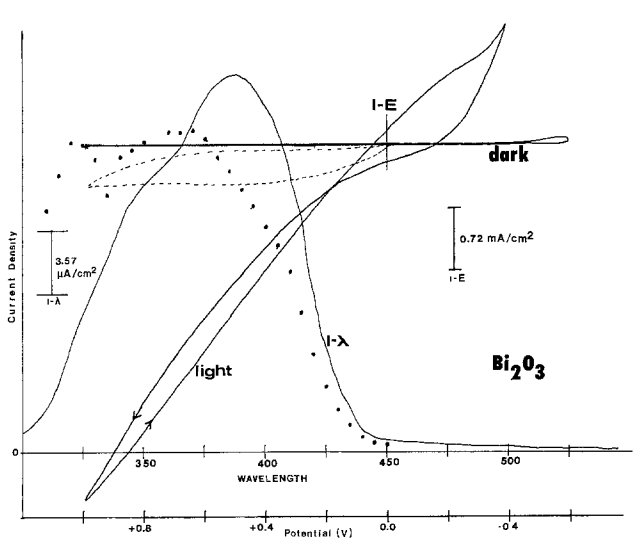

Fig. 12. Current *vs.* potential and current *vs.* wavelength curves for Bi_2O_3 in 0.25M Na_2SO_4 *p*H 8. $E = 0.80$V for *i-λ* curve. Current scale for corrected *i-λ* curve (···) is 2× value shown for uncorrected curve.

ratio was 60:40; after 45 min, the α:γ ratio was 90:10. Since these latter samples had less γ-Bi_2O_3 and showed lower photocurrents, the anodic photocurrent is probably attributable to the γ-Bi_2O_3.

X-ray examination of the electrode after the 1 hr illumination with subsequent decay in photocurrent and appearance of a yellow surface revealed no new forms of bismuth oxide. The x-ray data were not accurate enough to conclude whether or not the γ was converted to α-form, causing the photocurrent decay, or whether the yellow coating which could be a thin film of α-Bi_2O_3, was blocking the surface to further anodic photocurrents.

Unlike the other semiconductors, Bi_2O_3 exhibited both anodic and cathodic photocurrents. Bi_2O_3 has been reported to be an amphoteric semiconductor with n- and p-type behavior (12). It is not known how the presence of both the α- and γ-Bi_2O_3 affects the type of conductivity of the material. Figure 13 shows a cathodic i-E scan from 0.00V. The light was manually chopped during the course of the scan revealing the current to be a cathodic photocurrent, and not the result of the reduction of an anodically produced species (*e.g.*, O_2). The cathodic current is increased after an anodic scan with light, but the primary increase is a photosensitive one. The current becomes cathodic at about +0.2V and also responds to the chopping of the light. This cathodic photocurrent is probably due to the reduction of absorbed oxygen, while at more negative potentials reduction of the Bi_2O_3 also seems to occur. If the potential is held at −0.48V under illumination, a larger anodic dark current is seen similar to the dotted line in Fig. 12 upon a subsequent scan to positive potentials.

When the potential is scanned to −1.4V (Fig. 14), a large reduction peak at −1.05V *vs.* SCE is observed. Illumination shifts the peak to more positive potentials by about 0.1V and alters its shape slightly. The anodic dark current increased as a result of this scan and did not return to the low values initially present. The yellow color formed anodically under illumination disappeared after scanning over the reduction peak. It only reappeared with anodic scans and illumination, or in scans to large positive potentials, where oxygen evolution occurs, in the dark. The exact nature of this coating is, again, unknown as no x-ray peaks assignable to any other form of bismuth oxide were distinguishable.

The photocurrent *vs.* wavelength curves are given for both the anodic (Fig. 12b) and cathodic photocurrents (Fig. 13b). The onset of the photocurrent

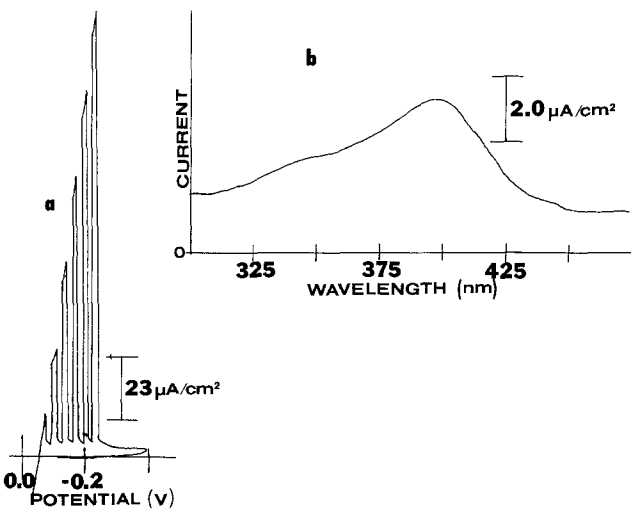

Fig. 13. (a) Current *vs.* potential curve for Bi_2O_3, chopped white light, in 0.25M Na_2SO_4, pH 9. (b) Current *vs.* wavelength for cathodic photocurrent; E = −0.475V *vs.* SCE.

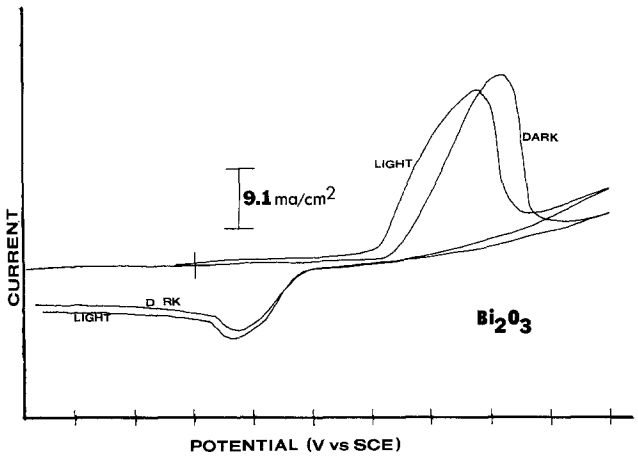

Fig. 14. Current *vs.* potential curve for Bi_2O_3 in 0.25M Na_2SO_4, pH 9.

occurs at about 450 nm (corresponding to an E_g of 2.8 eV) for both curves. The shape of the cathodic curve is not accurate because of the instability in the cathodic currents, and reduction of the oxide. The curve shape is similar to the anodic photocurrent curve, however. Note that the observed photoeffects cannot be ascribed to changes in photoconductivity of the Bi_2O_3 film, since the measured film resistance is low (a few ohms) and was not affected appreciably by illumination. The differences in semiconductor behavior between α- and γ-Bi_2O_3 are not known. The corrected anodic photocurrent *vs.* potential curve shows a steeper rise than those for Fe_2O_3 on TiO_2, possibly indicating a difference in transitions. Although Bi_2O_3 is not stable and has a bandgap only slightly smaller than that of TiO_2, it offers the interesting property of both n- and p-type behavior.

Tungsten oxide.—Hodes, Cahen, and Manassen (9) have observed photosensitized generation of oxygen at polycrystalline WO_3 electrodes prepared by oxidation of the metal or by decomposition of ammonium tungstate on glass. We have observed similar behavior at WO_3 electrodes made by heating W foil, thermally decomposing WCl_6 on Pt, and CVD of WO_3 on Pt. The i-E curves for all of these electrodes show quite similar behavior (Fig. 15). Unlike Hodes *et al.*, we found the anodic photocurrent at a W-foil electrode changed upon repetitive anodic scans with light. The photocurrent increased on each subsequent scan and two anodic peaks appeared at 0.2 and 0.4V *vs.* SCE. After these scans, the dark i-E scan showed a much higher anodic current (about one-half of the photocurrent) which showed the same peaks. This behavior could represent some further oxidation of the W foil or the oxide which, although nominally WO_3 by x-ray diffraction, is probably a nonstoichiometric form. This same behavior occurred for several different W-foil electrodes. The electrode surface was a deep blue before and after illumination. This behavior (appearance of peaks) was not observed for either of the WO_3-Pt electrodes. The photocurrent *vs.* time curves at E = 0.60V *vs.* SCE were quite stable for 10-20 min, with gas evolution observed. The photocurrent then gradually decayed. Examination of the surface revealed that parts of the electrode were bare Pt. Apparently the film had poor adhesion to the Pt. X-ray diffraction revealed the material on the Pt to be WO_3, but did not distinguish slight alterations in composition.

The differences in the oxide composition between the three types of electrodes are evident from the photocurrent *vs.* wavelengths curves (Fig. 15). All show an absorbency beginning at wavelengths corresponding to about 2.6 eV *vs.* the 2.8 eV reported as

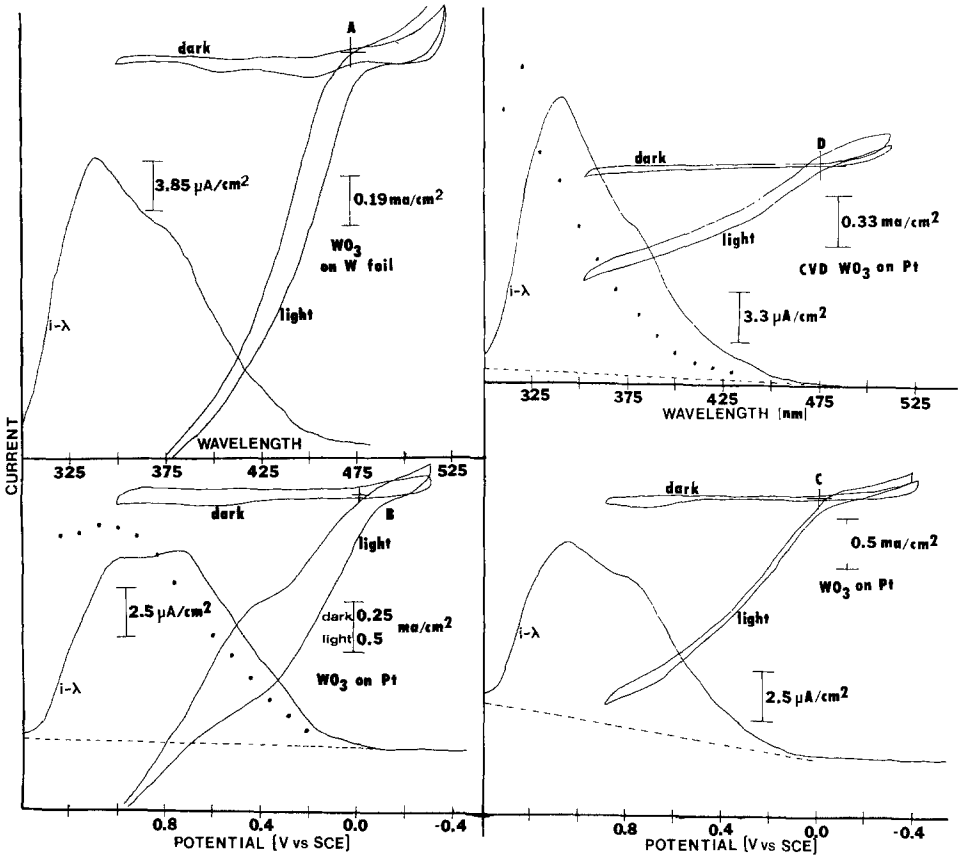

Fig. 15. Current *vs.* potential and current *vs.* wavelength curves for (a) WO_3 on W foil, 0.25M Na_2SO_4, *p*H 8; (b-c) WO_3 on Pt (formed from heating WCl_6 in EtOH solution), 0.25M Na_2SO_4, *p*H 9; (d) CVD WO_3 on Pt, 0.25M Na_2SO_4, *p*H 9. All *i*-λ curves at $E = 0.600$V *vs.* SCE. Corrected current scale is 2× uncorrected scale.

the bandgap of WO_3 (10). The shift in the peak location, similar to that observed by Hodes *et al.* (9), must represent structural or composition differences between the polycrystalline and single crystal materials.

Lead oxide.—Another metal oxide that has been found to exhibit photoelectrochemical effects is lead oxide; an *i-E* curve with a *p*H 9 0.25*M* Na_2SO_4 solution is shown in Fig. 16. The anodic dark current was usually low, although on some electrodes it was quite high initially but decreased to values shown in Fig. 16a or lower after illumination. With light a somewhat larger photocurrent was observed on the initial scan of a new electrode. The current then remained approximately constant on subsequent scans. The surface changed from an initial blue gray to a bronze brown color; this, coupled with the decrease in dark currents observed after illumination, indicates that at least part of the photocurrent contributes to further oxidation of the surface.

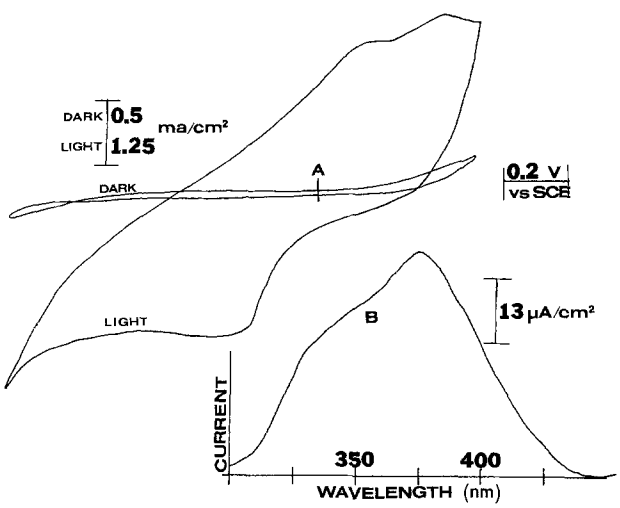

Fig. 16. Current *vs.* potential and current *vs.* wavelength curves for lead oxide in 0.25M Na_2SO_4, *p*H 9. $E = 0.600$V *vs.* SCE for *i*-λ curve.

After an anodic scan with light, the subsequent cathodic current was much higher, sometimes exceeding the anodic photocurrents. The cathodic current gradually decayed in the dark over several scans. It decayed rapidly when the potential was held at −0.2 to −0.4V. However, anodic scans under illumination again increased the subsequent cathodic current. A few gas bubbles were visible on the electrode surface under illumination, but the quantity was much less than that observed at TiO_2 or Fe_2O_3 at similar currents. Moreover, the magnitude of the cathodic current was too large to be accounted for by reduction of adsorbed oxygen. Both an anodic and cathodic transient response similar to those observed with Fe_2O_3 but present even under white light illumination were also found with lead oxide. This again is an indication of a reductive current causing an over-all loss in efficiency in the electrode.

Thus the anodic photocurrent is probably primarily that due to further oxidation of the electrode surface, while the cathodic current is the reduction of the newly formed oxide. X-ray diffraction examination performed on an electrode surface after prolonged illumination indicated the presence of Pb, PbO (litharge), PbO_2 (platernite), and Pb_3O_4 (minium). The bandgaps of these oxides are approximately 2.8, 2.0, and 2.1 eV, respectively (10). From the photocurrent *vs.* wavelength curve, Fig. 16b, a value of about 2.8 eV is obtained, suggesting that PbO is probably responsible for the photocurrent. PbO has been studied as a photoconductor in the solid state (13-15). According to Tennant (13), PbO is a photosensitizer with an absorption spectrum similar to what we observed at the PbO electrode (Fig. 16b). Thus the properties of the electrode are consistent with PbO and the other oxides are, then, the products of the photo-oxidation. The existence of other stable oxides offers a competing path for photo-oxidation of water at PbO

electrodes, compared to TiO_2 and Fe_2O_3 which have no such stable higher oxides. These preliminary experiments showing the reversible behavior of the lead oxide electrode, *i.e.*, photo-oxidation and dark reduction

$$PbO + 2\,OH^- \underset{\text{dark } (+2e)}{\overset{\text{light } (+2h^+)}{\rightleftharpoons}} PbO_2 + H_2O$$

suggest the interesting possibility of using a lead oxide electrode in a "photochargeable" battery. Moreover, PbO_2 has been used often as an electrode for the oxidation of organic compounds (17), so the PbO electrode might also be useful in photoelectrosynthesis. These possibilities are under investigation.

Copper oxide.—A typical *i-E* curve for a copper oxide electrode formed by the oxidation of $CuNO_3$ on Pt is shown in Fig. 17. For comparison, the *i-E* curve for a Pt foil of similar area in the same solution (0.25*M* Na_2SO_4, *p*H 6.7) is also given. X-ray diffraction of the oxide coating reveals it to be all CuO, which, as shown by the cathodic photoeffect, exhibits a p-type behavior. The onset of the photocurrent occurs at about 0.28V (*vs.* SCE), giving a potential shift of about 0.5V from the dark current rise at the same electrode. Both curves showed negative shifts in potential with increasing *p*H. The shapes of the dark and light curves are significantly different, suggesting that the photocurrent processes are not the same as those occurring during passage of the dark current. The dark current rise showed a hysteresis loop which usually indicates a change in the electrode surface. No loop is seen in the photocurrent curve, which is quite similar in shape to the *i-E* curve seen with the Pt electrode, where the cathodic current rise represents H^+ reduction and the resultant anodic peak on reversal is hydrogen oxidation.

No gas bubbles were seen at the CuO electrode under illumination. However, this could be the result of the relatively low currents and to the instability of the photocurrent. Over a 10 min period, the photocurrent decayed to approximately a quarter of its original value. The surface color changed from an initial black to a black interspersed with gold. Anodic dark scans after prolonged illumination revealed a larger anodic current similar to that in Fig. 17a. An x-ray diffraction pattern of the electrode after formation of the gold areas still revealed only CuO present, but some Pt was also found (~1%) where it had been absent before, indicating removal of some of the CuO.

The photocurrent *vs.* wavelength curve given in Fig. 18 shows a very wide spectral range for CuO, extending to about 700 nm corresponding to a bandgap of 1.7 eV. No literature value of the bandgap was found for comparison. The monochromatic photocurrent depended upon the stirring rate, indicating some diffusional nature to the photocurrent consistent with at least some H^+ reduction. The cathodic current in the dark probably represents reduction of the oxide, since it shows the hysteresis loop and occurs about 0.5V before the H^+ reduction on Pt. The cathodic photocurrent probably represents both H^+ and oxide reduction. The wide spectral range of CuO and its p-type behavior offer interesting possibilities in conjunction with an n-type electrode (*e.g.*, Fe_2O_3) for solar energy use, provided the apparent instability can be overcome.

Vanadium oxide.—Although V_2O_5 dissolves in aqueous solutions (acidic or alkaline), it was of interest to see if it also exhibited any photoeffect. Electrodes of single crystal and CVD material were used. The *i-E* and *i-λ* curves for both electrodes are given in Fig. 19. Onset of the photocurrent occurs at about 0.58V for CVD material and at about 0.8V for the single crystal. The crystal had a higher resistance (about 12 kohm) than the CVD electrode. Both *i-λ* curves are similar, although the CVD curve is broader in the shorter wavelength region. Both give an absorption edge of 450 nm corresponding to a bandgap of 2.75 eV, which is about the bandgap listed for V_2O_5 (10). The CVD electrode dissolved during use which probably affected the magnitude of the photocurrent, and thus the shape of the *i-λ* curve. The single crystal electrode, which was initially smooth, had striations in the surface after use. Because of its instability and the relatively low photocurrents observed, the processes giving rise to the photocurrent were not investigated further.

Other oxides.—Oxides of Cd, Co, Cr, Mn, and Sr were formed by CVD and by thermal decomposition of suitable solutions onto Pt substrates. No noticeable (at least a 10 μA difference between dark and light) photoeffects were observed for the oxides of Mn, Cd, or Sr. Oxide electrodes of Cr and Co exhibited low cathodic photocurrents superimposed on the dark currents. Both Cr_2O_3 and CoO have been reported to be p-type semiconductors (11). For Cr_2O_3 in *p*H 9, 0.25*M* Na_2SO_4, an approximately constant cathodic photocurrent of 45 μA/cm² (observed by manually chopping the light) was superimposed on a dark current of 0-150 μA/cm² (potential range, 0.0 to −0.80V).

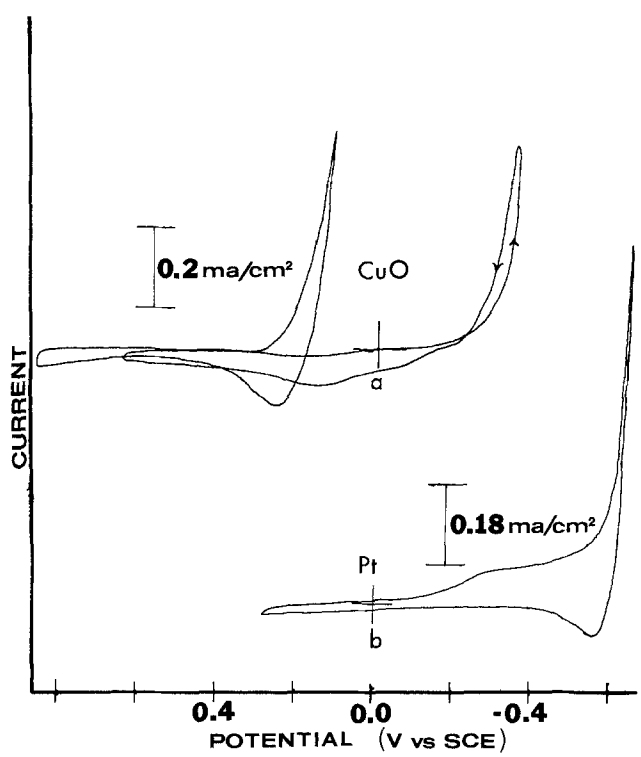

Fig. 17. Current *vs.* potential curve for (a) CuO and (b) Pt in 0.25M Na_2SO_4, *p*H 6.72.

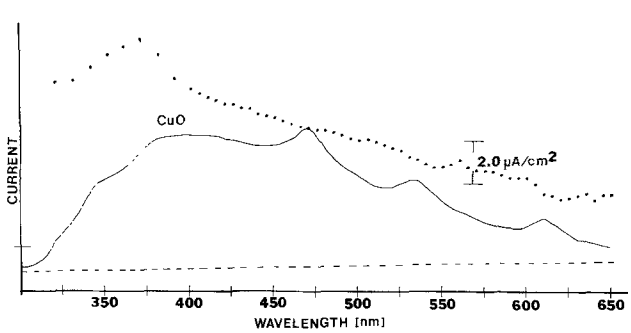

Fig. 18. Current *vs.* wavelength curve for CuO. $E = 0.00V$ *vs.* SCE, 0.25M Na_2SO_4, *p*H 6.72.

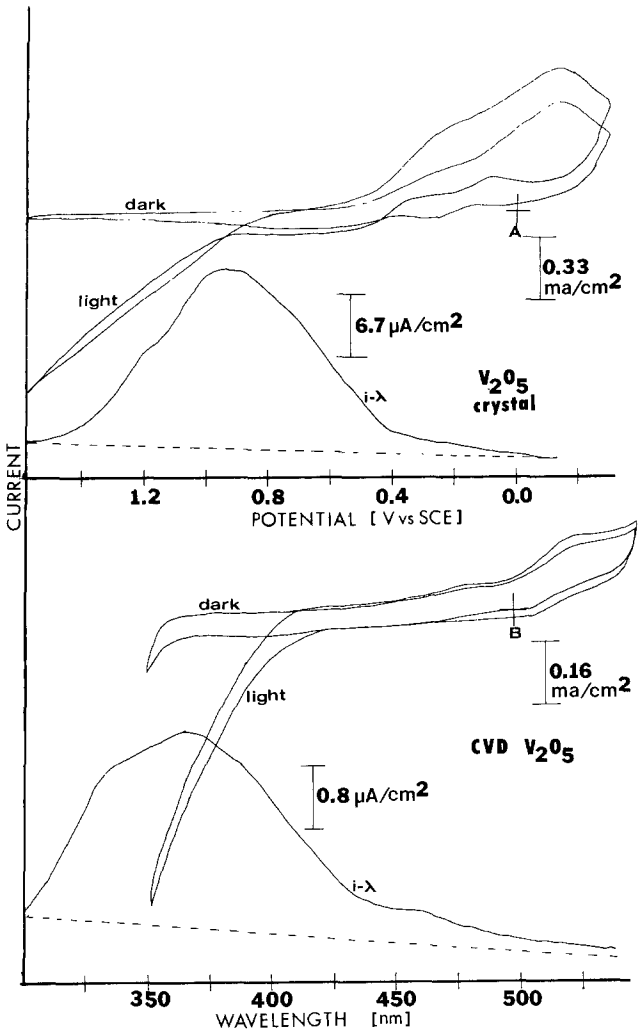

Fig. 19. Current vs. potential and current vs. wavelength curves in 0.5M Na_2SO_4 for (a) V_2O_5 single crystal, $E = 1.50V$ vs. SCE for i-λ curve; (b) CVD V_2O_5, $E = 1.00V$ vs. SCE for i-λ curve.

For CoO the photocurrent increased with potential. An instantaneous photocurrent of 0.2 mA/cm^2 at -0.90V was observed, superimposed on a dark current of 0.3 mA/cm^2. The current for these electrodes (in both dark and light) was not sufficiently stable with time to obtain good i-λ curves.

Conclusion

The results given here demonstrate that a number of metal oxides can be used as semiconductor electrodes which show photosensitized electrode reactions. Moreover, polycrystalline materials are useful for surveying promising semiconductor materials. Several methods (CVD, thermal decomposition of solutions, direct oxidation of metals, anodization, and sintering) can be employed with similar results. Thus, while single crystals are still valuable for detailed studies of the effect of structure on the photoeffect and fundamental studies of efficiency, information on the nature of the photocurrent and material stability can be easily gained from polycrystalline materials. For use in practical devices, good stability is required, including small tendency to dissolve directly or under illumination, stability against photo-oxidation (for n-type materials), and stability against photoreduction (for p-type materials). This stability depends upon the location of the valence band, but also upon the existence of higher or lower oxidation states.

Of the oxides examined only TiO_2, Fe_2O_3, and possibly WO_3 appeared to be stable enough for water oxidation. Only Fe_2O_3 offers stability and the relatively low bandgap needed for solar energy uses. None of the oxides examined seemed to have as negative a flatband potential as TiO_2. However, the shapes of most of the i-E curves did not exhibit the well-defined shape of that for TiO_2, making estimates of the actual flatband potential from the onset of the photocurrent difficult. Fe_2O_3, WO_3, Bi_2O_3, and PbO all showed an onset of photocurrent at approximately the same potential, indicating that the conduction band locations are about the same. One approach to finding useful materials may involve modification of the structure or composition of TiO_2, Fe_2O_3, and WO_3 by introduction of impurity bands or the formation of ternary compounds involving these.

Acknowledgments

The support of this research by the National Science Foundation (MPS74-23210) is gratefully acknowledged. We are indebted to Professor A. B. Scott for the sample of single crystal V_2O_5 and to Kay Poteet for assistance with x-ray and SEM analysis.

Manuscript submitted July 7, 1976; revised manuscript received Aug. 27, 1976.

Any discussion of this paper will appear in a Discussion Section to be published in the December 1977 JOURNAL. All discussions for the December 1977 Discussion Section should be submitted by Aug. 1, 1977.

Publication costs of this article were assisted by The University of Texas at Austin.

REFERENCES

1. K. L. Hardee and A. J. Bard, *This Journal*, **122**, 739 (1975).
2. K. L. Hardee and A. J. Bard, *ibid.*, **123**, 1024 (1976).
3. D. L. Laser and A. J. Bard, *ibid.*, **123**, 1837 (1976).
4. D. L. Laser and A. J. Bard, *ibid.*, **123**, 1027 (1976).
5. S. N. Frank and A. J. Bard, Submitted for publication.
6. B. Pettinger, H. R. Schoppel, and H. Gerischer, *Ber. Bunsenges. Phys. Chem.*, **78**, 450 (1974); *ibid.*, **78**, 1024 (1974).
7. R. F. G. Gardner, F. Sweett, and D. W. Tanner, *J. Phys. Chem. Solids*, **24**, 1175 (1963); *ibid.*, **24**, 1183 (1963).
8. F. Mollers, H. J. Tolle, and R. Memming, *This Journal*, **121**, 1160 (1974).
9. G. Hodes, D. Cahen, and J. Manassen, *Nature*, **260**, 312 (1976).
10. W. H. Strehlow and E. L. Cook, *J. Phys. Chem. Ref. Data*, **2**, 163 (1973).
11. "Transition Metal Oxides," NBS Report NSRDS 49.
12. H. Gobrecht, S. Seeck, H. E. Bergt, A. Martens, and K. Kossman, *Phys. Status Solidi*, **34**, 569 (1969).
13. W. C. Tennant, *J. Phys. Chem.*, **72**, 1078 (1968).
14. M. J. Shea and W. C. Michels, *J. Chem. Phys.*, **59**, 2764 (1973).
15. R. C. Keezer, D. L. Bowman, and J. H. Becker *J. Appl. Phys.*, **39**, 2062 (1968).
16. P. J. Boddy, *This Journal*, **115**, 199 (1968).
17. N. Sato, T. Sekine, and K. Sugino, *ibid.*, **115**, 242 (1968) and references therein.